Inorganic Chemistry
Article

Inorg. Chem. **2010**, *49*, 1337–1346 **1337**
DOI: 10.1021/ic9009674

Back-to-Back Dinuclear Platinum Terpyridyl Complexes: Synthesis and Photophysical Studies

Zhiqiang Ji, Suyue Li, Yunjing Li, and Wenfang Sun*

Department of Chemistry and Molecular Biology, North Dakota State University, Fargo, North Dakota 58108-6050

Received May 16, 2009

Two back-to-back terpyridine ligands using fluorenyl as bridging group (**1-L** and **2-L**) and their corresponding dinuclear platinum(II) complexes (**1** and **2**) were synthesized and characterized. Their electronic absorption, photoluminescence, and the triplet transient difference absorption were systematically investigated. Both ligands possess intense $^1\pi,\pi^*$ absorption in the UV region, and they exhibit structured $^1\pi,\pi^*$ fluorescence around 400 nm. With addition of *p*-toluenesulfonic acid to the ligands, both the absorption band and the emission band are red-shifted because of the increased electron-withdrawing ability of the protonated terpyridines and possible mixture of some intraligand charge transfer (ILCT) character. For complexes **1** and **2**, they both exhibit broad and strong absorption between 400 and 500 nm, which is assigned as the $^1\pi,\pi^*/^1$ILCT/^{1}MLCT (metal-to-ligand charge transfer) transition. The involvement of ^{1}ILCT in the lowest excited state is evident by the acid titration experiment of the ligands. At room temperature, the complexes exhibit dual emission that admixes fluorescence and phosphorescence from the $^{1,3}\pi,\pi^*/^{1,3}$ILCT/^{1,3}MLCT states. The assignment of the emitting states is based on the distinct emission lifetimes, different sensitivity to oxygen quenching, and different temperature dependency. Both complexes exhibit emission at 77 K, which is assigned as the mixture of $^3\pi,\pi^*/^3$MLCT. **1** and **2** also exhibit two triplet excited-state absorption bands in the visible to the NIR region, which are tentatively attributed to the $^3\pi,\pi^*$ and ^{3}MLCT/^{3}ILCT state. In addition, the connection pattern between the fluorenyl component and the terpyridyl components influences the excited-state characteristics of both the ligands and the complexes. Ligand **1-L** and its corresponding platinum complex **1** that have the triplet bond connection between the fluorenyl and terpyridyl components exhibit a red-shifted low-energy absorption band, an emission band, and a transient absorption band compared to ligand **2-L** and complex **2** that have the fluorenyl directly attached to terpyridyl components. These differences could be rationalized by the enhanced conjugation between the fluorenyl and terpyridyl components in **1-L** and **1** because of the better coplanarity induced by the triple bond.

Introduction

Mononuclear square-planar platinum terpyridyl (tpy) complexes show intriguing spectroscopic properties and exhibit potential applications in materials science and biomedical field. Recent research revealed that platinum terpyridyl complexes could be utilized as photosensitizers for dye sensitized solar cell[1] and for singlet oxygen generation;[2] and highly emissive platinum complexes showed the potential for light emitting diode application.[3] Studies on applying platinum terpyridyl complexes as DNA intercalators,[4] antitumor drugs,[5] chemical and biomolecule sensors,[6]

*To whom correspondence should be addressed. E-mail: wenfang.sun@ndsu.edu. Phone: 701-231-6254. Fax: 701-231-8831.

(1) (a) Chakraborty, S.; Wadas, T. J.; Hester, H.; Flaschenreim, C.; Schmehl, R.; Eisenberg, R. *Inorg. Chem.* **2005**, *44*, 6284. (b) Chakraborty, S.; Wadas, T. J.; Hester, H.; Schmehl, R.; Eisenberg, R. *Inorg. Chem.* **2005**, *44*, 6865.

(2) Zhang, D.; Wu, L. Z.; Yang, Q. Z.; Li, X. H.; Zhang, L. P.; Tung, C. H. *Org. Lett.* **2003**, *5*, 3221.

(3) (a) Lu, W.; Mi, B.-X.; Chan, M. C. W.; Hui, Z.; Che, C.-M.; Zhu, N.; Lee, S.-T. *J. Am. Chem. Soc.* **2004**, *126*, 4958. (b) Yersin, H.; Donges, D.; Humbs, W.; Strasser, J.; Sitters, R.; Glasbeek, M. *Inorg. Chem.* **2002**, *41*, 4915. (c) Brooks, J.; Babayan, Y.; Lamansky, S.; Djurovich, P. I.; Tsyba, I.; Bau, R.; Thompson, M. E. *Inorg. Chem.* **2002**, *41*, 3055. (d) Shi, J. C.; Chao, H. Y.; Fu, W. F.; Peng, S. M.; Che, C. M. *J. Chem. Soc., Dalton Trans.* **2000**, *18*, 3128. (e) Chassot, L.; von Zelewsky, A.; Sandrini, D.; Maestri, M.; Balzani, V. *J. Am. Chem. Soc.* **1986**, *108*, 6084. (f) Maestri, M.; Sandrini, D.; Balzani, V.; Chassot, L.; Jolliet, P.; von Zelewsky, A. *Chem. Phys. Lett.* **1985**, *122*, 375. (g) Wong, W.-Y.; He, Z.; So, S.-K.; Tong, K.-L.; Lin, Z. *Organometallics* **2005**, *24*, 4079.

(4) (a) Lippard, S. *Acc. Chem. Res.* **1978**, *11*, 211. (b) Clark, M. L.; Green, R. L.; Johnson, O. E.; Fanwick, P. E.; McMillin, D. R. *Inorg. Chem.* **2008**, *47*, 9410.

(5) (a) Ma, D. L.; Shum, T. Y. T.; Zhang, F. Y.; Che, C. M.; Yang, M. S. *Chem. Commun.* **2005**, 4675. (b) Lowe, G.; Droz, A. S.; Vilaivan, T.; Weaver, G. W.; Park, J. J.; Pratt, J. M.; Tweedale, L.; Kelland, L. R. *J. Med. Chem.* **1999**, *42*, 3167.

(6) (a) Wong, K. M. C.; Tang, W. S.; Lu, X. X.; Zhu, N.; Yam, V. W. W. *Inorg. Chem.* **2005**, *44*, 1492. (b) Han, X.; Wu, L.-Z.; Si, G.; Pan, J.; Yang, Q.-Z.; Zhang, L.-P.; Tung, C.-H. *Chem.—Eur. J.* **2007**, *13*, 1231. (c) Wong, K. M. C.; Tang, W. S.; Chu, B. W. K.; Zhu, N.; Yam, V. W. W. *Organometallics* **2004**, *23*, 3459. (d) Lo, H. S.; Yip, S. K.; Wong, K. M. C.; Zhu, N.; Yam, V. W. W. *Organometallics* **2006**, *25*, 3537. (e) Wadas, T. J.; Wang, Q. M.; Kim, Y. J.; Flaschenreim, C.; Blanton, T. N.; Eisenberg, R. *J. Am. Chem. Soc.* **2004**, *126*, 16841.

Published on Web 01/21/2010

and as catalysts for hydrogen production[7] have been reported as well. In addition, recent research in our group demonstrated that platinum terpyridyl complexes could be promising broadband nonlinear transmission materials.[8]

The spectroscopic properties of dinuclear platinum terpyridyl complexes are more interesting because the possible intramolecular Pt−Pt and $\pi-\pi$ interactions in the dinuclear complexes could tune the electronic absorption and luminescence properties. An earlier work by Gray and co-workers[9] reported that colors of a series of binuclear platinum terpyridine complexes changed to darker color and the emission maxima moved to lower energy with decreasing Pt−Pt separation. Nishihara and co-workers[10] reported the pendant type dinuclear platinum complexes with anthraquinone as a spacer. The two Pt(tpy) components were fixed in a side-by-side geometry with short Pt−Pt distance. Thus, a lower-energy absorption band and emission band from intramolecular metal−metal-to-ligand charge transfer (MMLCT) state were observed for these molecules. Yam and co-workers described that acetamidate-bridged dinuclear platinum terpyridyl complex exhibited distinctive solid state emission depending on the crystal packing pattern,[11] which resulted in different degrees of metal−metal and $\pi-\pi$ interactions. In another work, Yam and co-workers reported the influence of the length of the conjugated alkynyl bridging ligand on the photophysical properties of the dinuclear platinum terpyridyl complexes [Pt]-$(C\equiv C)_n$-[Pt]. When the number of n increased from 1 to 3, both the lowest-energy absorption band and the emission band blue-shifted. No Pt−Pt interactions were clearly evident in these complexes. Lowe and co-workers[5b] investigated the cytotoxicity of several dinuclear terpyridyl platinum complexes against human ovarian carcinoma and found that the cytotoxicity of these dinuclear complexes depended strongly on the nature of the linker. The dinuclear complex with a flexible linker showed poor cytotoxicity, while the dinuclear complexes with rigid and short linkers are highly effective. The aforementioned works are all interesting; however, most of the reported work on the dinuclear platinum complexes used a rigid bridging ligand to form a face-to-face geometry. To date, the reports on the dinuclear platinum terpyridyl complexes with a back-to-back geometry are scarce. Except for the work reported by Lowe and co-workers on the poor cytotoxicity of one dinuclear platinum terpyridyl complex with flexible linker at the 4′-position of the terpyridine ligands,[5b] Yam and co-workers studied the photophysical properties of a series of dinuclear platinum complexes with flexible polyethyleneglycol bridge at the 4′-position of the tpy ligands.[12] They found that the conformation of the dinuclear complexes with appropriate-length bridge could change from "side-by-side" arrangement at low temperatures to "back-to-back" arrangement at high temperatures, which would result in the switch of the lowest excited state from MMLCT at low temperatures to MLCT at high temperatures. In these two papers, flexible bridging ligands were used to connect the two Pt(tpy) components; thus, no electronic interaction between the bridging ligand and the Pt(tpy) components was observed. Although Schmehl et al.,[13] Harriman and Lehn et al.,[14] and Harriman and Ziessel et al.[15] reported the electron delocalization in polyene or phenyl or ethynyl bridged binuclear ruthenium or osmium diimine complexes, and a study on the delocalization of MLCT excited states by rigid bridging ligands in dinuclear ruthenium terpyridine complexes was reported by Hammarström, Barigelletti, Collin, Sauvage and co-workers,[16] so far no study on the influence of the conjugated rigid bridging ligands on the photophysical properties of the back-to-back dinuclear platinum complexes has been carried out. To the best of our knowledge, the only work currently available in the literature on the "back-to-back" dinuclear platinum terpyridyl complexes was the synthesis of one dinuclear platinum complex using a 1,4-didodecyloxy-benzene as the bridging ligand.[17]

To understand the influence of conjugated rigid bridging ligands on the photophysics of the "back-to-back" dinuclear platinum complexes, we have designed and synthesized two ditopic terpyridine ligands (**1-L** and **2-L**) and their dinuclear platinum complexes (**1** and **2**, shown in Chart 1). The two terpyridine units are attached on the 2,7-position of a fluorene group directly or through a carbon−carbon triple bond. Therefore, no intramolecular Pt−Pt and $\pi-\pi$ interactions are expected. The fluorene unit is chosen as the bridging ligand because of its synthetic convenience, π-donating ability, and high emission efficiency. Therefore, the two ligands (**1-L** and **2-L**) are expected to be highly emissive; and after coordination with platinum some degree of intraligand charge transfer from the fluorene unit to the (tpy)-$PtCl^+$ components is anticipated to occur. In addition, the highly conjugated ligand could possibly lower the π,π^* state either as the lowest excited state or in close proximity to other excited states, such as MLCT and/or ILCT. All these would render rich photophysics to the synthesized platinum complexes **1** and **2**. For comparison purpose, the photophysics of the corresponding ligand is also studied.

Experimental Section

Synthesis. All solvents were purchased from VWR Scientific Company with analytical grade, and used without further purification unless otherwise stated. All of the chemicals and silica gel (230−400 mesh) were purchased from Alfa Aesar Company. 2,7-Dibromofluorene (**3**),[18] 2,7-dibromo-9,9-dioctylfluorene (**4**),[19] 4-(7-(3-hydroxy-3-methyl-but-1-ynyl)-9,9-dioctyl-9*H*-fluoren-2-yl)-2-methyl-but-3-yn-2-ol (**5**),[20]

(7) Du, P. W.; Schneider, J.; Jarosz, P.; Eisenberg, R. *J. Am. Chem. Soc.* **2006**, *128*, 7726.
(8) (a) Sun, W.; Wu, Z.-X.; Yang, Q.-Z.; Wu, L.-Z.; Tung, C.-H. *Appl. Phys. Lett.* **2003**, *82*, 850. (b) Sun, W.; Guo, F. *Chin. Opt. Lett.* **2005**, *S3*, S34. (c) Guo, F.; Sun, W. *J. Phys. Chem. B* **2006**, *110*, 15029. (d) Pritchett, T. M.; Sun, W.; Guo, F.; Zhang, B.; Ferry, M. J.; Rogers-Haley, J. E.; Shensky, W.; Mott, A. G. *Opt. Lett.* **2008**, *33*, 1053. (e) Ji, Z.; Li, Y.; Sun, W. *Inorg. Chem.* **2008**, *47*, 7599.
(9) Bailey, J. A.; Miskowski, V. M.; Gray, H. B. *Inorg. Chem.* **1993**, *32*, 369.
(10) Utsuno, M.; Yutaka, T.; Murata, M.; Kurihar, M.; Tamai, N.; Nishihara, H. *Inorg. Chem.* **2007**, *46*, 11291.
(11) Wong, K. M. C.; Zhu, N. Y.; Yam, V. W. W. *Chem. Commun.* **2006**, 3441.
(12) Yam, V. W.-W.; Chan, K. H.-Y.; Wong, K. M.-C.; Chu, B. W.-K. *Angew. Chem., Int. Ed.* **2006**, *45*, 6169.
(13) Baba, A. I.; Ensley, H. E.; Schmehl, R. H. *Inorg. Chem.* **1995**, *34*, 1198.
(14) Benniston, A. C.; Goulle, V.; Harriman, A.; Lehn, J.-M.; Marczinke, B. *J. Phys. Chem.* **1994**, *98*, 7798.
(15) Grosshenny, V.; Harriman, A.; Romero, F. M.; Ziessel, R. *J. Phys. Chem.* **1996**, *100*, 17472.
(16) Hammarström, L.; Barigelletti, F.; Flamigni, L.; Indelli, M. T.; Armaroli, N.; Calogero, G.; Guardigli, M.; Sour, A.; Collin, J.-P.; Sauvage, J.-P. *J. Phys. Chem. A* **1997**, *101*, 9061.
(17) Ziessel, R.; Diring, S. *Tetrahedron Lett.* **2006**, *47*, 4687.
(18) Sung, H. H.; Lin, H. C. *Macromolecules* **2004**, *37*, 7945.
(19) Potts, K. T.; Konwar, D. *J. Org. Chem.* **1991**, *56*, 4851.
(20) Chen, Y.-Y.; Tao, Y.-T.; Lin, H.-C. *Macromolecules* **2006**, *39*, 8559.

Chart 1. Structures of **1-L**, **2-L**, **1**, and **2**

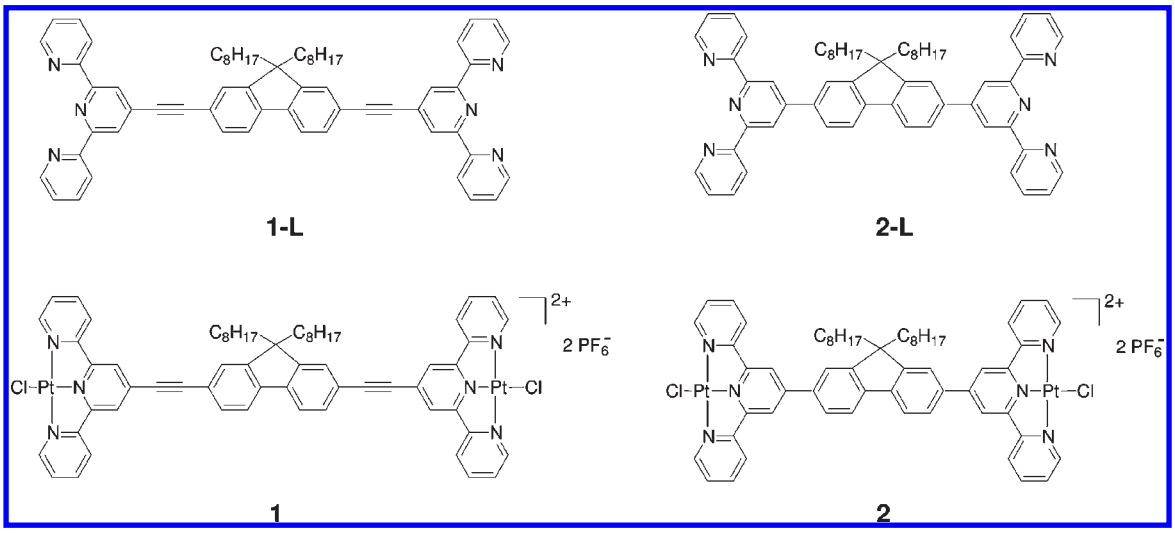

2,7-diethynyl-9,9-dioctyl-9*H*-fluorene (**6**),[19] and 2,7-di(pinacolboronicester)fluorene (**7**)[21] were all synthesized according to the literature procedures. All products were characterized by ^{1}H NMR, elemental analysis, and high-resolution MS. ^{1}H NMR spectra were obtained using a Varian 400 or 500 MHz VNMR spectrometer. Elemental analyses were conducted by NuMega Resonance Laboratories, Inc. in San Diego, CA. High resolution MS data were obtained using a Bruker BioTof III mass spectrometer.

1-L. Compound **6** (0.53 g, 1.21 mmol) and 4′-trifluoromethylsulfonyloxy-2,2′:6′,2″- terpyridine (1.01 g, 2.65 mmol) were added to a 20 mL mixture of benzene and di(*iso*-propyl)amine (v/v = 1:1). The mixture was degassed at room temperature for 20 min and $Pd(PPh_3)_4$ (170 mg, 0.17 mmol) was added. The mixture was heated to reflux under argon for overnight. After the solvent was removed, the residue was purified on neutral Al_2O_3 column twice. The column was first eluted by 10:1 hexane/dichloromethane to remove the unreacted 4′-trifluoromethylsulfonyloxy-2,2′:6′,2″-terpyridine, and then by 1:1 hexane/dichloromethane to give the crude product. The crude product was recrystallized in CH_2Cl_2/hexane to give 435 mg pale yellow needles in 42% yield. ^{1}H NMR ($CDCl_3$, 400 MHz): δ 8.72 (4H, d, J = 4.0 Hz), 8.63−8.61 (8H, m), 7.86 (4H, dt, J = 8.0, 1.5 Hz), 7.71 (2H, d, J = 8.5 Hz), 7.57−7.55 (4H, m), 7.36−7.33 (4H, m), 2.03−1.99 (4H, m), 1.20−1.08 (20H, m), 0.78 (6H, t, J = 7.2 Hz), 0.65 (4H, m). HRMS (m/z): calcd for $[C_{63}H_{60}N_6+H]^+$, 901.4952; found, 901.4981 (100%). Anal. Calcd for $C_{63}H_{60}N_6$: C, 83.96; H, 6.71; N, 9.33. Found: C, 83.95; H, 6.42; N, 9.41.

1. $Pt(DMSO)_2Cl_2$ (42.2 mg, 0.10 mmol) and $AgCF_3SO_3$ (25.7 mg, 0.10 mmol) were added in 3 mL of dimethylsulfoxide (DMSO). The mixture was stirred at room temperature for 24 h, and the white solid was filtered out. The filtrate was heated to 100 °C, and **1-L** (45.0 mg, 0.05 mmol) was added. The mixture was kept at 100 °C for 2 h. After cooling to room temperature, excess amount of saturated NH_4PF_6 aqueous solution was added. The mixture was stirred at room temperature for 1 h, and then the red solid was collected by centrifugation. After recrystallization in DMF/Et_2O, 36.5 mg of a red solid was obtained in 44% yield. ^{1}H NMR (d_6-DMSO, 400 M Hz): δ 0.49 (4H, br, s), 0.73 (6H, t, J = 7.0 Hz), 0.92−1.19 (20H, m), 2.09 (4H, m), 7.72 (2H, d, J = 8.0 Hz), 7.83 (2H, s) 7.99 (4H, t, J = 6.0 Hz), 8.09 (2H, d, J = 8.0 Hz), 8.54 (4H, t, J = 8.0 Hz), 8.69 (4H, d, J = 8.0 Hz), 8.89 (4H, s), 8.98 (4H, d, J = 5.6 Hz). HRMS (m/z): calcd for $[C_{63}H_{60}N_6Pt_2Cl_2]^{2+}$, 681.1770; found, 681.1774 (100%). Anal. Calcd for $C_{63}H_{60}N_6Pt_2Cl_2P_2F_{12}$: C, 45.80; H, 3.66; N, 5.09. Found: C, 45.91; H, 4.02; N, 5.45.

2-L. Compound **7** (321 mg, 0.50 mmol) and 311 mg of 4-bromo-2,2′:6′,2″-terpyridine (312 mg, 1.00 mmol) were added to 30 mL of toluene. A 2.5 mL portion of 2 M K_2CO_3 aqueous solution was added. The mixture was degassed in argon for 30 min. $Pd(PPh_3)_4$ (46 mg, 0.05 mmol) was added. The mixture was heated to reflux under argon for overnight. After the solvent was removed, the residue was purified on neutral Al_2O_3 column. The unreacted 4′-bromo-2,2′:6′,2″-terpyridine was removed first by using 10:1 hexane/CH_2Cl_2 as the eluent, and the crude product was obtained by elution using toluene. After recrystallization from CH_2Cl_2/hexane, 220 mg of a colorless crystals was obtained as the pure product (yield: 52%). ^{1}H NMR ($CDCl_3$, 400 MHz): δ 0.56 (4H, m), 0.71 (6H, t, J = 6.4 Hz), 0.98−1.15 (20H, m), 2.12−2.16 (4H, m), 7.34−7.37 (4H, m), 7.85−7.92 (10H, m), 8.67 (4H, d, J = 8.0 Hz), 8.74 (4H, d, J = 4.4 Hz), 8.78 (4H, s). HRMS (m/z): calcd for $[C_{59}H_{60}N_6+H]^+$, 853.4952; found, 853.4962 (100%). Anal. Calcd for $C_{59}H_{60}N_6$: C, 83.06; H, 7.09; N, 9.85. Found: C, 83.42; H, 6.70; N, 10.03.

2. $Pt(DMSO)_2Cl_2$ (42.2 mg, 0.10 mmol) and $AgCF_3SO_3$ (25.7 mg, 0.10 mmol) were added in 3 mL of DMSO. The mixture was stirred at room temperature for 24 h., and the white solid was filtered out. The filtrate was heated to 100 °C, and **2-L** (42.6 mg, 0.05 mmol) was added. The mixture was kept at 100 °C for 2 h. After cooling to room temperature, excess amount of saturated NH_4PF_6 aqueous solution was added. The mixture was stirred at room temperature for 1 h, and the yellow solid was collected by centrifugation. The pure product was obtained by recrystallization in DMF/Et_2O to afford 36.7 mg yellow solid (yield: 46%). ^{1}H NMR (d_6-DMSO, 400 MHz): δ 0.76 (10H, m), 1.11 (20, t, J = 6.0 Hz), 2.20 (4H, m), 8.01 (4H, t, J = 6.8 Hz), 8.29 (2H, d, 8.0 Hz), 8.38 (2H, d, J = 8.0 Hz), 8.46 (2H, s), 8.60 (4H, t, J = 8.0 Hz), 8.91 (4H, d, J = 8.0 Hz), 9.02 (4H, d, J = 8.4 Hz), 9.06 (4H, s). HRMS (m/z): calcd for $[C_{59}H_{60}N_6Pt_2Cl_2]^{2+}$ 656.6768; found, 656.6782. (100%) Anal. Calcd for $C_{59}H_{60}N_6Pt_2Cl_2P_2F_{12}$: C, 44.18; H, 3.77; N, 5.24. Found: C, 43.89; H, 3.76; N, 5.60.

Photophysical Studies. The electronic absorption spectra were recorded on a Shimadzu 2501 PC UV−vis spectrophotometer. Complexes **1** and **2** were dissolved in CH_3CN, and ligands **1-L** and **2-L** were dissolved in CH_2Cl_2. The steady-state emission spectra at room temperature and 77 K were all recorded on a SPEX Fluorolog-3 fluorometer/phosphorometer. **1** and **2** were dissolved in CH_3CN, and **1-L** and **2-L** were dissolved in CH_2Cl_2 for room temperature measurement. The low temperature

(21) Cho, S. Y.; Grimsdale, A. C.; Jones, D. J.; Watkins, S. E.; Holmes, A. B. *J. Am. Chem. Soc.* **2007**, *129*(39), 11910.

Scheme 1. Synthetic Routes for Complexes **1** and **2**

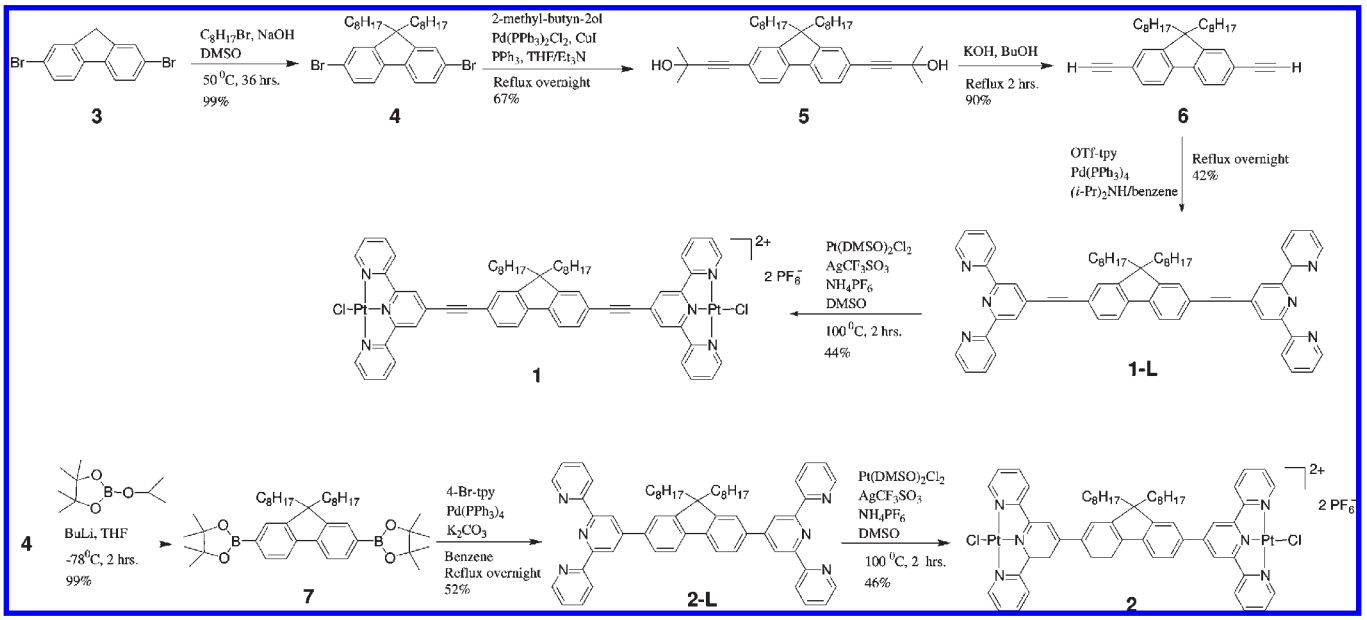

(77 K) emission was measured in butyronitrile glassy matrix. Solutions were degassed for 30 min prior to each measurement. The emission lifetimes were measured on an Edinburgh LP920 laser flash photolysis spectrometer. The excitation was provided by the third-harmonic output (355 nm) of a Quantel Brilliant Q-switched Nd:YAG laser (fwhm pulsewidth was 4.1 ns and the repetition rate was set at 1 Hz). The sample solutions were degassed for 30 min before each measurement. The emission lifetimes of **1-L** and **2-L** in CH_2Cl_2 with and without *p*-TsOH were measured by time-correlated single photon counting (TCSPC) technique. Samples were excited at 375 nm with a 70 ps pulse, and the decay of the emission was monitored at their respective emission band maximum. The emission quantum yields of **1-L**, **2-L**, **1**, and **2** were determined by the comparative method.[22] A degassed aqueous solution of $[Ru(bpy)_3]Cl_2$ ($\phi_{em} = 0.042$, excited at 436 nm)[23] was used as the reference for complexes **1** and **2**; and anthracene in ethanol ($\phi_{em} = 0.27$)[24] was the reference for the ligands **1-L** and **2-L**.

The triplet transient difference absorption spectra were measured on the Edinburgh LP920 laser flash photolysis spectrometer. The excitation was provided by the third-harmonic output (355 nm) of the Quantel Brilliant Q-switched Nd:YAG laser (fwhm pulsewidth was 4.1 ns and the repetition rate was set at 1 Hz). The solutions were degassed for 30 min before each measurement. The absorbance of the solution was adjusted to $A = 0.4$ at 355 nm in a 1 cm quartz cuvette.

Electrochemical Measurements. The redox potentials of complexes **1** and **2** were measured by cyclic voltammetry on an Epsilon electrochemical workstation (BASi EC epsilon potentiostat) in *N*,*N*-dimethylformamide (DMF). The supporting electrolyte was 0.1 M tetrabutylammonium hexafluorophosphate (TBAPF6), and ferrocene was used as the internal standard. The solutions were purged with Ar for 15 min prior to each measurement. The working electrode, counter electrode, and reference electrode were Au, Pt, and $Ag/AgNO_3$, respectively.

Results and Discussion

Synthesis. The synthetic routes for **1-L**, **2-L**, **1** and **2** are shown in Scheme 1. 2,7-Dibromofluorene (**3**) was synthesized according to the literature procedure,[18] which then reacted with 1-bromooctane in NaOH/DMSO solution to yield 2,7-dibromo-9,9′-dioctylfluorene (**4**) in a quantitative yield. The two octyl chains were introduced to the fluorenyl group to improve the solubility of the final complexes **1** and **2**. Double Sonogashira cross-coupling reactions of 2,7-dibromo-9,9′-dioctylfluorene and 2-methyl-3-butyn-2-ol in the presence of $Pd(PPh_3)_2Cl_2$ and CuI generated compound **5** in 67% yield, which was deprotected by heating in the presence of KOH to give compound **6** in 90% yield. Compound **6** reacted with 4′-trifluoromethylsulfonyloxy-2,2′:6′,2″-terpyridine in the presence of catalytical amount of $Pd(PPh_3)_4$ to form **1-L** in 42% yield.

2-L was also synthesized from the same starting material 2,7-dibromo-9,9′-dioctylfluorene (**4**). 2,7-Dibromo-9,9′-dioctylfluorene was converted to borate ester by reaction with BuLi and 2-*iso*-propoxy-4,4,5,5-tetramethyl-1,3,2-dioxaborolane. **2-L** was obtained by Suzuki coupling reaction of 2,7-di(pinacolboronicester)fluorene and 4′-bromo-2,2′:6′,2″-terpyridine with catalytical amounts of $Pd(PPh_3)_4$ in 52% yield. It is worth to note that great care should be taken to purify both **1-L** and **2-L** through recrystallization in CH_2Cl_2/hexane after column chromatography to obtained high purity compounds for the photoluminescence study to eliminate the emission from impurity.

The synthesis of **1** was attempted in two ways by using **1-L** with two different platinum salts. The coordination reaction was first conducted by reaction of **1-L** and $Pt(DMSO)_2Cl_2$ in degassed $CHCl_3$. However, HRMS analysis showed that no product was formed. In another attempt, a highly reactive platinum salt was prepared by exchange of one chloride coligand in $Pt(DMSO)_2Cl_2$ with 1 equiv of $AgCF_3SO_3$ in DMSO. After filtration of AgCl, one-half molar equivalent of **1-L** and the reaction solution were heated at 100 °C for 2 h. Pure complex **1** was achieved by recrystallization in DMF/Et_2O with a 44% yield. **2** was synthesized following the same procedure as that for **1** with a 46% yield. All the synthesized ligands

(22) Demas, J. N.; Crosby, G. A. *J. Phys. Chem.* **1971**, *75*, 991.
(23) Van Houten, J.; Watts, R. J. *J. Am. Chem. Soc.* **1976**, *98*, 4853.
(24) Melhuish, W. H. *J. Phys. Chem.* **1961**, *65*, 229.

and complexes were characterized by ^{1}H NMR, HRMS, and elemental analysis.

Electronic Absorption. The electronic absorption spectra of **1-L**, **2-L**, **1**, and **2** are shown in Figure 1, and the absorption band maxima and extinction coefficients are summarized in Table 1. Within the concentration range of 5×10^{-6}−1×10^{-4} mol/L, the absorption of all samples obeys the Beer−Lambert law, indicating that no ground-state aggregation occurs. **1-L** displays two major absorption bands at 285 and 361 nm, with a shoulder appearing at 377 nm; while **2-L** only displays absorption at 288 and 339 nm. Although the $^1\pi,\pi^*$ transitions of the individual terpyridine and fluorene all fall below 300 nm, the strong absorption band above 300 nm for each of these compounds suggests that electronic coupling occurs between the fluorene component and the two terpyridine components; and the coupling is stronger in **1-L** than in **2-L** in view of the much red-shifted low-energy band in **1-L**. The weaker coupling in **2-L** should be attributed to the nonplanar geometry between the fluorene and the terpyridyl components that arises from the steric hindrance between the 1,3-hydrogens on fluorene and the 3′-hydrogen on terpyridine, which would decrease the effective conjugation length in **2-L**. In contrast, the triple bonds in **1-L** allow for the terpyridine adopting a more coplanar geometry with the fluorene unit and thus enhance the conjugation in **1-L**. Consequently, the low-energy band shifts to a longer wavelength for **1-L**.

Because the terpyridine components in **1-L** and **2-L** are basic, they can act as Lewis bases to coordinate with transition metal ions like Pt^{2+} and can also be protonated. In either case, the electron density on the terpyridine components would be decreased, which would affect the electronic absorption of **1-L** and **2-L** accordingly. To understand how the protonation influences the electronic absorption of **1-L** and **2-L**, acid-titration of **1-L** and **2-L** has been conducted, and the results are shown in Figure 2. For **1-L**, upon addition of *p*-TsOH, the absorption band at 361 nm gradually decreases, accompanied by an increase of the absorption at 418 nm. After addition of 4 equiv of *p*-TsOH, no further change of the spectrum occurs. The appearance of the 418 nm band could be attributed to two factors: first, the protonation of the terpyridine nitrogen atoms would decrease the electron density on the compound, which would stabilize the π^*

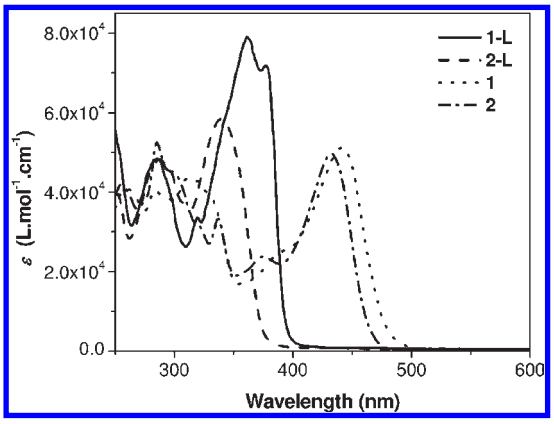

Figure 1. Electronic absorption spectra of **1-L** and **2-L** in CH_2Cl_2, and **1** and **2** in CH_3CN.

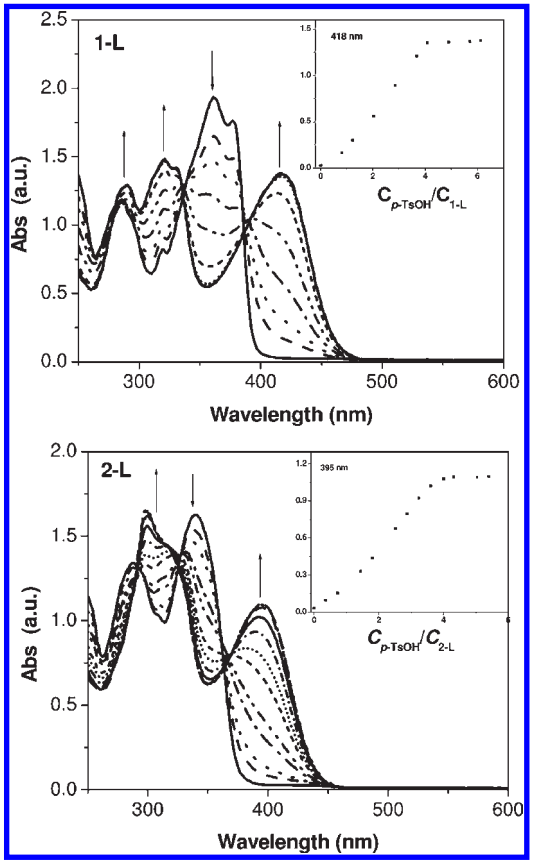

Figure 2. UV−vis spectra of **1-L** and **2-L** with addition of *p*-TsOH in CH_2Cl_2. ($c = 2.5 \times 10^{-5}$ mol/L for **1-L** and 2.8×10^{-5} mol/L for **2-L**).

Table 1. Photophysical Parameters of **1-L**, **2-L**, **1**, and **2**

		λ_{em}/nm (τ/μs; Φ_{em}, k_r/s^{-1}), R.T.		λ_{em}/nm (τ/μs) [e]
	λ_{abs}/nm (ε/L mol^{-1} cm^{-1})	in CH_3CN[c]	in CH_2Cl_2[d]	77 K
1-L	285 (48380), 320 (33510), 361 (79020), 377 (71850)[a]		389, 405 (690 ps; 0.99)	
1-L-H	290 (51560), 321 (58910),[a] 418 (54650)		550 (660 ps (20%), 2260 ps (80%))	
1	259 (41000), 284 (40600), 312 (43200), 390 (25000), 440 (51200)[b]	598 (1.6; 0.0078; 4.4×10^3)	611 (9.4; 0.073; 1.4×10^4)	588 (98), 632 (94)
2-L	288 (48250), 339 (58480)[a]		374, 388 (880 ps; 0.88)	
2-L-H	299 (59300), 395 (39210)[a]		512 (570 ps (5%), 5380 ps (95%))	
2	255 (41810), 285 (52500), 337 (33300), 374 (23830), 431 (49580)[b]	587 (1.65; 0.011; 5.8×10^3)	594 (6.5; 0.121; 7.6×10^4)	564 (81), 609 (78)

[a] Electronic absorption band maxima and molar extinction coefficients in CH_2Cl_2 solutions; [b] Electronic absorption band maxima and molar extinction coefficients in CH_3CN solutions; [c] Room temperature emission band maxima and decay lifetimes measured at a concentration of 5×10^{-5} mol/L, and emission quantum yields measured at solutions with $A_{436} = 0.1$ in CH_3CN solutions; [d] Emission in CH_2Cl_2 at a concentration of 1×10^{-5} mol/L. [e] Emission band maxima and decay lifetimes in butyronitrile glassy solutions at 77 K; the concentration of the solution is 3×10^{-5} mol/L.

Table 2. Solvent-Dependent Electronic Absorption and Emission Data of **1** and **2** ($c = 1 \times 10^{-5}$ mol/L)

complex		CH_2Cl_2	THF	CH_3CN	MeOH	DMF
1	λ_{abs}/nm	462	451	440	441	439
	λ_{em}/nm	611	602	598	597	594
	τ_{em}[a]/ns	9400	158	1600	135	
	Φ_{em}	0.073	0.0032	0.0078	0.0044	0.0032
2	λ_{abs}/nm	446	443	432	433	440
	λ_{em}/nm	594	592	587	584	589
	τ_{em}[a]/ns	6500	182	1650	117	100
	Φ_{em}	0.12	0.0018	0.011	0.0019	0.0014

[a] The lifetimes were measured at the emission band maxima.

orbital of the compound and consequently reduce the energy of the π,π^* transition; second, the increased electron-accepting ability of the protonated terpyridine would likely induce intramolecular charge transfer from the electron-rich fluorene component to the electron-deficient protonated terpyridine components. This would also result in a low-energy absorption band. However, the UV−vis absorption spectrum in different solvents reveals that minor solvent effect is present for **1-L** (Supporting Information, Figure S1). Considering the minor solvent effect and the high extinction coefficient for the 418 nm band of the acidified ligand **1-L**, this band could be assigned as a $^1\pi,\pi^*$ transition, possibly mixed with some charge transfer character. The similar results were obtained for **2-L** upon acidification (shown in Figure 2 and Supporting Information, Figure S1).

The electronic absorption spectra of the dinuclear platinum complexes **1** and **2** in Figure 1 reveal that they also exhibit strong $^1\pi,\pi^*$ transitions in the UV region. In addition, like the acidified ligands discussed in the previous paragraph, **1** and **2** possess intense absorption bands at 440 and 431 nm, respectively. In view of the similar energies of these bands to those of their corresponding acidified ligands, and the similar energy to the MLCT band in Pt(4′-Pyrel-T)Cl^+ complex,[25] it is likely that these bands contain $^1\pi,\pi^*$, ^{1}ILCT, and ^{1}MLCT characters. The involvement of the $^1\pi,\pi^*$ character in these bands is supported by the much larger extinction coefficients of these bands than those for typical MLCT or ILCT transitions; it is also reflected by the much smaller solvatochromic shift of this band compared to a typical charge transfer band. As summarized in Table 2 and shown in Supporting Information, Figure S2, the lowest-energy absorption bands for **1** and **2** show a negative solvatochromic effect (namely, in low polarity solvents, such as CH_2Cl_2, this band appears at a longer wavelength; while in more polar solvents, such as CH_3CN, the band shows a hypsochromic shift). Although the solvatochromic shifts in **1** and **2** are much less than a typical solvatochromic shift for charge transfer transitions, the negative solvatochromic effect still clearly indicates the involvement of charge-transfer character in this low-energy absorption band.

Electrochemical Properties. Cyclic voltammetric studies were carried out in DMF solution to obtain the redox potentials for complexes **1** and **2**, and the results are summarized in Table 3. Both complexes exhibit two

Table 3. Redox Potentials of **1** and **2** in DMF

	oxidation[a]	reduction[b]
complex	E_{pa}/V vs Fc/Fc^+	$E_{1/2}$/V vs Fc/Fc^+
1	0.91	−1.09, −1.69
2	0.72	−1.12, −1.80

[a] E_{pa} refers to the anodic peak potential for the irreversible oxidation wave. [b] $E_{1/2} = (E_{pa} + E_{pc})/2$, where E_{pa} and E_{pc} are the respective anodic and cathodic peak potential.

quasi-reversible reduction peaks at about −1.10 and −1.75 V vs $Fc^{+/0}$, which agree well with those of Pt(4′-Ar-T)Cl^+ complexes reported in the literature.[25] Therefore, these peaks could be attributed to the terpyridine-based reduction. The slightly less negative reduction potentials of **1** compared to those of **2** could possibly arise from the stronger electron-withdrawing ability of the sp carbon on the triple bond in comparison to that of the sp^2 carbon on the fluorenyl ring although the better electron-delocalization in **1** than in **2** could counteract this σ-bonding interaction. An irreversible oxidation peak is observed at 0.91 V (vs $Fc^{+/0}$) for **1** and 0.72 V (vs $Fc^{+/0}$) for **2**, which are much lower than those reported for metal-centered oxidation from Pt(II) to Pt(III) in the platinum terpyridyl acetylide complexes reported by Yam et al.[26] and Wu et al.[27] (1.02−1.56 V vs SCE). In contrast, these values are comparable to the oxidation potentials for fluorene-containing fullerene triads in *o*-dichlorobenzene (∼0.80 V vs Fc/Fc^+),[28] in which electron-transfer from fluorene to fullerene occurs. Therefore, the oxidation peaks in **1** and **2** could be tentatively assigned as the fluorene-based oxidation. This indicates that charge transfer from the fluorene component to the terpyridine components could occur in **1** and **2**, which partially supports the ILCT assignment for the lowest energy absorption band in the UV−vis absorption spectra as discussed in the previous section. The higher oxidation potential of **1** than that of **2** could also be related to the stronger electron-withdrawing effect of the triple bond carbon through σ-bonding interaction.

Photoluminescence. 1-L and **2-L** are highly emissive at room temperature, with an emission quantum yield of 99% and 88% in CH_2Cl_2, respectively (Table 1). The emission spectra (Figure 3) are essentially mirror-image to their low-energy absorption bands with small Stokes shifts, and the lifetimes are less than 1 ns. Thus, the observed emission for these two ligands emanates from a singlet excited state, likely to be the $^1\pi,\pi^*$ state. This assignment is supported by the structured emission and the minor solvent effect on the fluorescence energy in different polarity solvents (Figure 4), which are characteristics of π,π^* emission. Because the fluorescence spectra are structured, excitation spectra were monitored at each of the emission band. The results show that the excitation spectra are identical when monitored at different emission wavelengths (see Supporting Information,

(25) Michalec, J. F.; Bejune, S. A.; Cuttell, D. G.; Summerton, G. C.; Gertenbach, J. A.; Field, J. S.; Haines, R. J.; McMillin, D. R. *Inorg. Chem.* **2001**, *40*, 2193.

(26) Yam, V. W.-W.; Tang, R. P.-L.; Wong, K. M.-C.; Cheung, K.-K. *Organometallics* **2001**, *20*, 4476.

(27) Yang, Q.-Z.; Wu, L.-Z.; Wu, Z.-X.; Zhang, L.-P.; Tung, C.-H. *Inorg. Chem.* **2002**, *41*, 5653.

(28) Sandanayaka, A. S. D.; Araki, Y.; Ito, O.; Deviprasad, G. R.; Smith, P. M.; Rogers, L. M.; Zandler, M. E.; D'Souza, F. *Chem. Phys.* **2006**, *325*, 452.

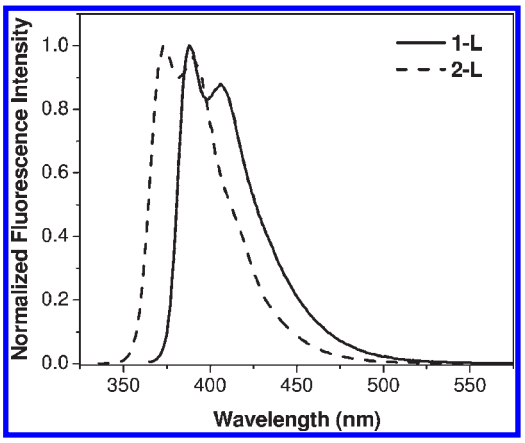

Figure 3. Normalized fluorescence spectra of **1-L** and **2-L** in CH_2Cl_2 at room temperature. The excitation wavelength was 361 nm for **1-L** and 333 nm for **2-L**.

Figure S3 for **1-L**). This indicates that the emission arises from the same excited state. Consistent with the trend observed in their electronic absorption spectra, the emission of **1-L** appears at a lower energy than that of **2-L**. This is the result of the more delocalized electronic structure of **1-L**.

The concentration-dependent fluorescence study was carried out for **1-L** and **2-L** to figure out if any inner-filter effect, ground-state aggregation, or self-quenching occurs at higher concentrations, which is important for future device applications. As shown in the Supporting Information, Figure S4, the fluorescence intensity of **1-L** increases from the concentration of 2.4×10^{-6} mol/L to 4.9×10^{-6} mol/L; however, the intensity starts to decrease at the concentration of 2.4×10^{-5} mol/L with the ratio of intensity at 405 nm over that at 389 nm increase. The similar result was observed for **2-L**, with the fluorescence intensity starting to decrease at the concentration of 5.2×10^{-5} mol/L (Supporting Information, Figure S4). The quenching of the fluorescence intensity and the change of the relative intensity ratio for **1-L** and **2-L** at high concentrations could be attributed to two factors: first, the absorbance at the excitation wavelength, that is, 361 nm for **1-L** and 333 nm for **2-L**, at the highest concentration used for study is quite high (>3), which would block the excitation source and thus decrease the emission; second, there is significant ground-state absorption at 389 nm for **1-L** and considerable absorption at 374 nm for **2-L**; this could reabsorb the emission (i.e., inner-filter effect) at these wavelengths and change the relative intensity ratio of the two apexes. In addition, the contribution from the self-quenching effect could not been ruled out.

To understand how the acidification of terpyridine components influences the emission of the ligands, emission from the acidified ligands **1-L** and **2-L** has been studied. As exemplified in Figure 5 for **2-L**, with the addition of *p*-TsOH, the original fluorescence band gradually decreases, while a new band at 512 nm increases until 2 equiv of acids were added. Excitation spectrum monitored at this new emission band reveals that this emission mainly emanates from a transition at about 395 nm, which is consistent with the $^1\pi,\pi^*/^1$ILCT transition in the UV−vis absorption spectrum (Supporting Information, Figure S5). The emission at 512 nm exhibits

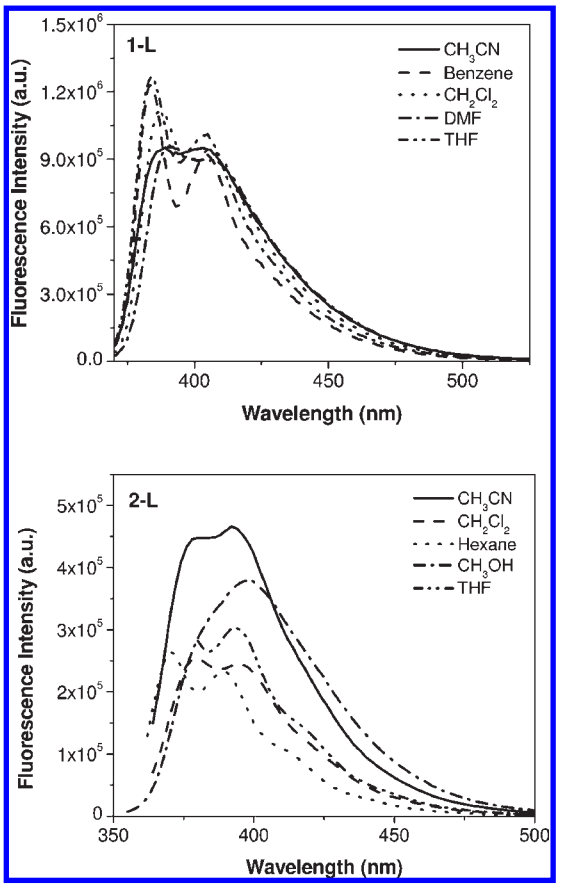

Figure 4. Solvent-dependent fluorescence spectra of **1-L** ($c = 1 \times 10^{-5}$ mol/L, $\lambda_{ex} = 361$ nm) and **2-L** ($c = 5 \times 10^{-6}$ mol/L, $\lambda_{ex} = 333$ nm) at room temperature.

biexponential decays, with a shorter lifetime of 570 ps that is in line with the $^1\pi,\pi^*$ emission of **2-L**, and a longer one of 5380 ps. Considering the large Stokes shift (~3725 cm^{-1}) of this emission band, the structureless feature, the excitation spectrum, and the biexponential decays, the emission at 512 nm for acidified **2-L** could be tentatively assigned as an ^{1}ILCT emission, likely mixed with some $^1\pi,\pi^*$ character. Similar results are observed for **1-L** as well, with the new emission band appearing at about 550 nm after protonation (Supporting Information, Figure S6).

Figure 6 displays the emission spectra of the dinuclear complexes **1** and **2** in CH_3CN. The spectra for both complexes are quite broad, with shoulders at both the longer and the shorter wavelengths and the band maximum appearing at 598 nm for **1** and 587 nm for **2**. These shoulders become more apparent in CH_2Cl_2 solutions, which will be discussed further in the following paragraph. The emission lifetimes monitored at the band maximum are of the order of microseconds, indicating that the emission at these wavelengths likely arises from a triplet excited state. This notion is supported by the large Stokes shifts for **1** and **2**. As listed in Table 2, the emission energy, lifetime, and quantum yield are influenced by the nature of the solvent, that is, both the polarity and the coordination ability of the solvent affect the emission characteristics. In noncoordinating, less polar solvents, such as CH_2Cl_2, the emission shifts to a lower energy and exhibits a prolonged lifetime and higher quantum yield in

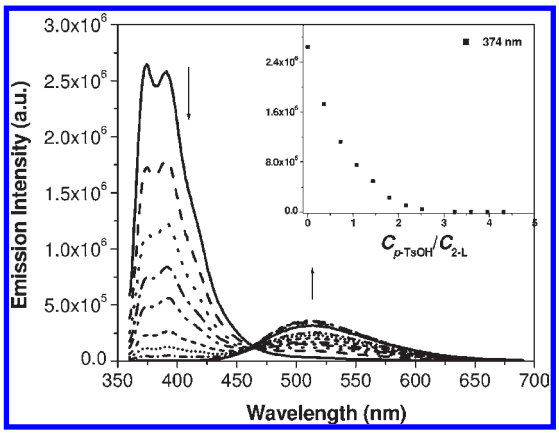

Figure 5. Room temperature emission spectra of **2-L** with addition of *p*-TsOH in CH_2Cl_2. λ_{ex} = 333 nm, $c = 2.8 \times 10^{-5}$ mol/L.

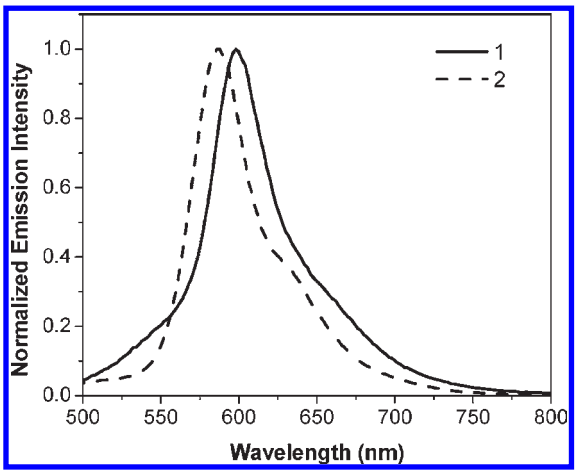

Figure 6. Normalized room temperature emission spectra of **1** (λ_{ex} = 440 nm) and **2** (λ_{ex} = 431 nm) in CH_3CN ($c = 1 \times 10^{-5}$ mol/L).

comparison to those in polar, coordinating solvents, such as CH_3CN. This negative solvatochromic effect implies that the emitting state has some charge-transfer character, and the quenching of the emission in coordinating solvent like CH_3CN, DMF, tetrahydrofuran (THF), and methanol, suggests that the emitting state has Pt metal involved. Considering these facts and the similar emission energy to that of the ^{1}ILCT/$^1\pi,\pi^*$ emission observed in the acidified ligand, we can tentatively attribute the emitting state to a mixture of ^{1,3}MLCT/^{1,3}ILCT in nature, possibly with large degree of involvement from the $^{1,3}\pi,\pi^*$ configurations in view of the long emission lifetime and the insignificant solvent effect on the emission energy comparing to a typical charge-transfer emitting state. The assignment of the emitting state to a mixture of multiple configurationally distinct excitations has been proposed by McMillin et al. to explain the long-lived emission of Pt(4′-pyrel-T)Cl^+;[25] and the involvement of the singlet MLCT, ILCT, and π,π^* characters in the emitting state will be further discussed in the following paragraph. In line with the reduced emission quantum yield in coordinating solvents (CH_3CN, DMF, THF, and methanol), the emission lifetimes in these solvents are significantly shorter than that in noncoordinating solvent CH_2Cl_2. This drastic difference in lifetime should be attributed to solvent-induced exciplex quenching,[25] which is commonly seen in transition-metal complexes with a MLCT emitting state. However, the quenching in CH_3CN is much less than in the other coordinating solvents like DMF, THF, and methanol. This probably reflects the different percentages of participation of the ILCT character in the emitting state. The suppression of solvent-induced exciplex quenching by incorporation of ILCT character into the MLCT state was previously reported by McMillin et al. for Pt(4′-pyrel-T)Cl^+[25] and Pt(4′-NMe_2-T)Cl^+.[29]

As mentioned earlier the emission spectra of **1** and **2** in CH_3CN exhibit two shoulders at both the shorter and the longer wavelengths of the band maximum, which is more salient in CH_2Cl_2 than in CH_3CN solution. To understand whether the emission at the shoulders has the same origin as that at the band maximum, excitation spectra of **1** in CH_2Cl_2 were monitored at emission wavelengths of 560, 610, and 668 nm, respectively. As shown in Figure 7, the excitation spectra monitored at 610 and 668 nm are almost identical, with the dominant excitation arising from the 466 nm band, which is almost the same energy as the $^1\pi,\pi^*$/^{1}ILCT/^{1}MLCT transition in its electronic absorption spectrum. Moreover, the vibronic spacing between the 610 and 688 nm band is approximately 1420 cm^{-1}, which is in accord with the aromatic vibrational mode of the terpyridyl ligands. In contrast, the emission at 560 nm is dominated by the $^1\pi,\pi^*$ excitation at 382 nm. The different nature of the emission at 560 nm from that at 610 and 668 nm is supported by three other pieces of evidence. First, the emission at 610 and 668 nm is significantly quenched in air-saturated solution, whereas the relative intensity at 560 nm remains the same (Figure 7), which indicates that the 560 nm emission is from a state that is insensitive to O_2, namely, a singlet excited state. Second, the emission lifetime at 560 nm (5.8 ns) is drastically different from those at 610 and 668 nm (9.4 and 9.0 μs, respectively). As shown in Supporting Information, Figure S7, the time-resolved emission spectrum of **1** exhibits distinct decay characters at 560 and 610 nm. The much shorter lifetime at 560 nm is clearly indicative of a singlet excited state. Third, the temperature dependency emission study reveals that the emission intensity at 560 nm remains essentially the same with decreased temperature, while the emission at 610 nm increases when the temperature is decreased (Figure 8). Furthermore, the aforementioned observation and analysis are consistent with what reported by McMillin et al. for Pt(4′-pyrel-T)Cl^+.[25]

Although the emission energies for **1** and **2** are independent of the concentration of solution, the emission intensity decreases at higher concentrations as exemplified by **1** in Figure 9. However, the emission lifetime remains almost the same at different concentrations, indicating that no self-quenching occurs at higher concentrations. Because no appreciable ground-state absorption occurs above 550 nm for **1**, neither can the quenching of emission be ascribed to the inner-filter effect. Instead, because of the very high absorbance at the excitation wavelength of 440 nm at high concentrations (i.e., 2.56 for the concentration of 5×10^{-5} mol/L and 5.12 for 1×10^{-4} mol/L), the quenching of the emission should be

(29) Crites, D. K.; McMillin, D. R. *Coord. Chem. Rev.* **2001**, *211*, 195.

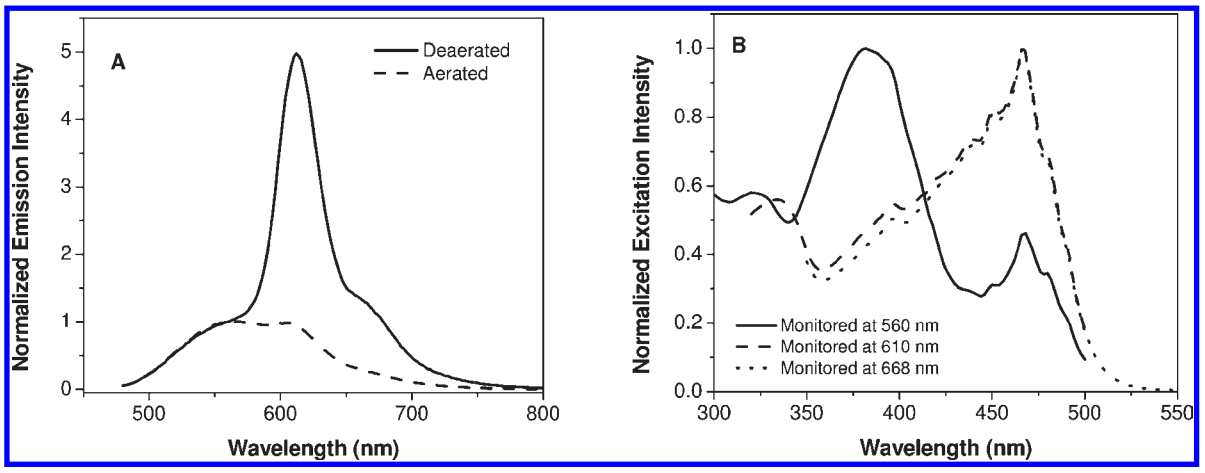

Figure 7. (A) Normalized emission spectra of **1** in air and argon saturated CH_2Cl_2 solutions at room temperature. λ_{ex} = 440 nm. (B) Excitation spectra of **1** in argon saturated CH_2Cl_2 solution monitored at different emission wavelengths.

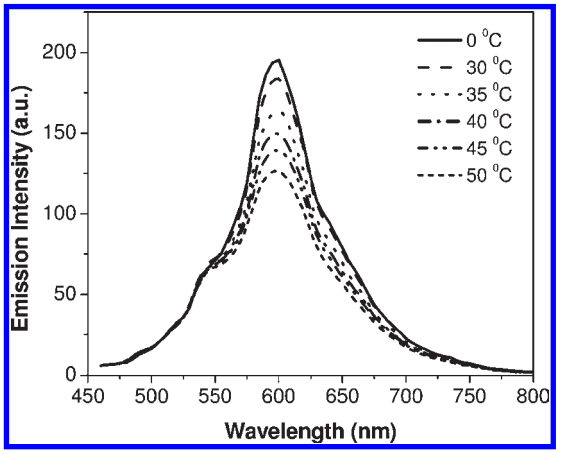

Figure 8. Temperature dependency emission of **1** in CH_3CN. λ_{ex} = 440 nm, $c = 1 \times 10^{-5}$ mol/L.

attributed to the blocked excitation, which results in the diminished emission.

The emission of **1** and **2** at 77 K was studied in butyronitrile solutions. The data are summarized in Table 1, and the concentration-dependent emission of **1** is shown in Figure 9. Both complexes exhibit long-lived (i.e., 98 μs for **1** and 81 μs for **2**) structured emission. The emission appears at 588 and 632 nm for **1** and 564 and 609 nm for **2** at a concentration of 3×10^{-5} mol/L. In line with the trend observed in their electronic absorption and room temperature emission, the emission energy at 77 K also shifts to lower energies for **1** compared to those of **2**. The vibronic spacing between the two bands is 1147 and 1311 cm^{-1} for **1** and **2**, respectively, which is consistent with the aromatic vibrational mode of the terpyridyl ligands. The emission is slightly blue-shifted compared to that at the room temperature, with the thermally induced Stokes shift (ΔE_s) being 284 and 695 cm^{-1} for **1** and **2** respectively. The vibronic structure, small value of ΔE_s, and the long lifetime indicate that the emission should stem from the $^3\pi,\pi^*$ state, possibly mixed with some ^{3}MLCT characters. As shown in Figure 9, the emission intensity increases from 1.8×10^{-6} mol/L to 3.7×10^{-5} mol/L, then decreases at a higher concentration of 7.4×10^{-5} mol/L, accompanied by a slight red-shift. The red-shift is also observed in the 3.7×10^{-5} mol/L

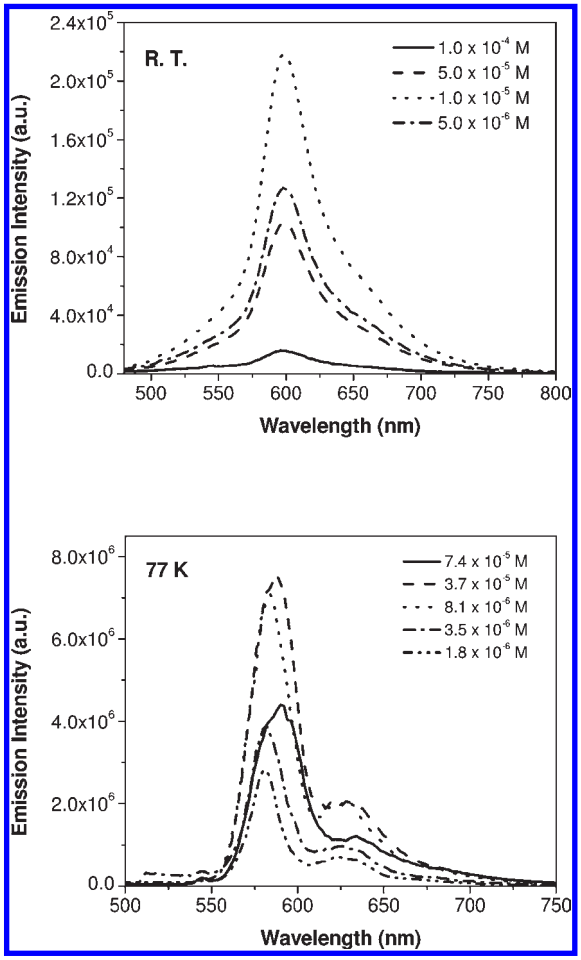

Figure 9. Concentration-dependent emission of **1** in CH_3CN at room temperature and in butyronitrile glassy solution at 77 K. λ_{ex} = 440 nm.

solution. However, no significant changes occur for the emission lifetime at the different concentrations. Therefore, the decrease of the emission intensity and the slight red-shift of the emission energy could be attributed to the formation of ground-state aggregation at higher concentrations. In addition, the blocked excitation because of the high absorbance at the excitation wavelengths in high-concentration solutions could also diminish the emission.

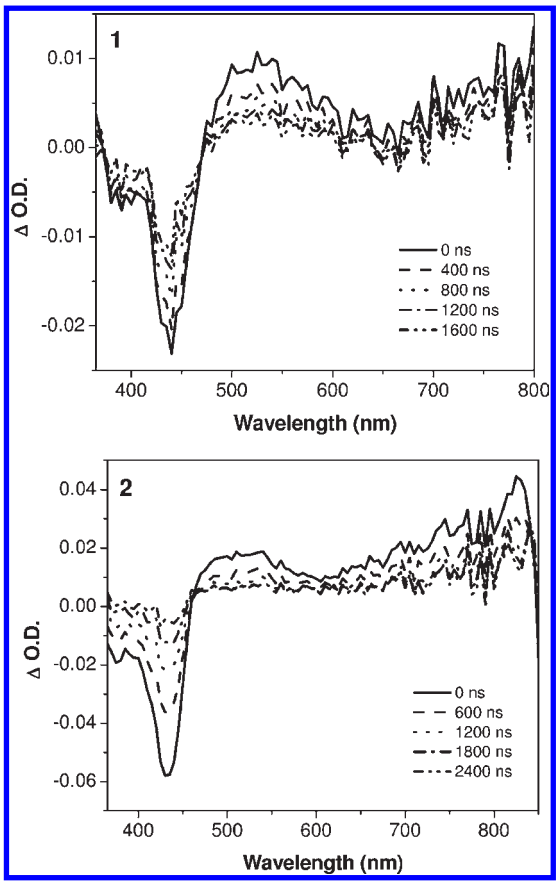

Figure 10. Time-resolved triplet transient difference absorption spectra of **1** and **2** in CH_3CN. λ_{ex} = 355 nm. The time shown in the legend is the time delay after excitation.

Triplet Transient Difference Absorption (TA). To further understand the excited-state properties, the triplet transient absorption of **1** and **2** in CH_3CN was studied. Figure 10 shows the time-resolved triplet transient difference absorption spectra of **1** and **2**. The spectral features for these two complexes are quite similar, with a bleaching band occurring below 470 nm and two broad, structureless absorption bands in the visible to the NIR region. The bleaching bands are consistent with the lowest-energy absorption band in their respective UV−vis absorption spectrum. The lifetimes obtained from the decay of the bleaching band of the triplet transient absorption in CH_3CN are 1.6 μs for both **1** and **2**, which is in accord with the lifetimes measured from the decay of the emission. These facts suggest that the triplet transient absorption possibly arises from the same excited state that emits or a state in equilibrium with the emitting state. Thus, this state possibly consists of $^3\pi,\pi^*$, ^{3}MLCT, and/or ^{3}ILCT characters. Further piece of evidence supporting the involvement of $^3\pi,\pi^*$ character in the transients arises from the transient absorption measurement of the ligands **1-L** and **2-L** in the presence of excess CH_3I (Supporting Information, Figure S8), in which broader absorption bands at ~580 nm for **1-L** and 550 nm for **2-L** are observed. These bands lie in the similar regions as the bands between 450 and 600 nm for **1** and **2**, respectively. In addition, it has been reported that the $^3\pi,\pi^*$ state of fluorene absorbs in the range of 400−600 nm.[30] Therefore, the absorption band between 450 and 600 nm likely arises from the $^3\pi,\pi^*$ state of the ligand. The involvement of the $^3\pi,\pi^*$ absorption of the bridging ligand has been reported by Schmehl et al. for bimetallic ruthenium diimine complexes with a conjugated bridging ligand.[13] On the other hand, the broad absorption band in the NIR region (between 600 and 800 nm) is the typical absorption band involving a ^{3}MLCT state according to the study reported by Castellano et al.[31]

Conclusion

The ditopic terpyridine ligands exhibit $^1\pi,\pi^*$ absorption and strong fluorescence in the UV/visible region. The dinuclear platinum complexes with these ditopic ligands as the bridge show intense absorption in the visible region, which is assigned as the $^1\pi,\pi^*/^1$ILCT/^{1}MLCT transition. The origin of the emission for these two complexes at room temperature are tentatively assigned to a mixture of six configurationally distinct excitations $^{1,3}\pi,\pi^*/^{1,3}$ILCT/^{1,3}MLCT in view of the distinct lifetimes, different sensitivities to oxygen, different temperature effect, and different solvent quenching effects at the high-energy shoulder and at the apex. At 77 K, the structured emission and the long lifetime suggest a mixed $^3\pi,\pi^*/^3$MLCT emission. For both the ligands and the platinum complexes, the ones with the triple bond connection (**1-L** and **1**) exhibit red-shifted absorption and emission compared to **2-L** and **2**, respectively, indicating that stronger electronic coupling between the two terpyridine components and the fluorene component because of the more coplanar geometry. **1** and **2** also exhibit two broad absorption bands in their triplet transient difference absorption spectra, which are tentatively attributed to a $^3\pi,\pi^*$ and ^{3}MLCT/^{3}ILCT state. These photophysical studies clearly indicate that the lowest excited states are primarily localized on the bridging ligand, with some mixture of the ILCT and MLCT characters. In addition, the drastic UV−vis absorption change and the emission energy and intensity changes upon acidification of the ligands suggest that these compounds could be potentially used as acid sensors.

Acknowledgment. We would like to acknowledge the National Science Foundation (CAREER CHE-0449598) and North Dakota State EPSCoR (ND EPSCoR Instrumentation Award) for financial support. We are also grateful to Dr. Joy Haley at UES Inc. and the Air Force Research Laboratory for measuring the excited-state lifetimes of the ligands **1-L** and **2-L**.

Supporting Information Available: The electronic absorption spectra of **1-L**, **2-L** and **1** in different solvents, the excitation spectra of **1-L** monitored at different emission wavelengths in CH_2Cl_2, the concentration-dependent emission spectra of **1-L** and **2-L** in CH_2Cl_2, the excitation spectrum of acidified CH_2Cl_2 solution of **2-L** at room temperature, the room temperature emission and excitation spectra of **1-L** with addition of *p*-TsOH in CH_2Cl_2, the time-resolved emission spectra of **1** in CH_2Cl_2 monitored at different time regime after excitation, and the triplet transient difference absorption spectra of **1-L** and **2-L** in the presence of excess CH_3I in CH_2Cl_2. This material is available free of charge via the Internet at http://pubs.acs.org.

(30) Canabate Diaz, B.; Schulman, S. G.; Carretero, A. S.; Fernadez Gutierrez, A. *Anal. Chim. Acta* **2003**, 165.

(31) Shikhova, E.; Danilov, E. O.; Kinayyigit, S.; Pomestchenko, I. E.; Tregubov, A. D.; Camerel, F.; Retailleau, P.; Ziessel, R.; Castellano, F. N. *Inorg. Chem.* **2007**, *46*, 3038.